Inorganic Chemistry

Article

pubs.acs.org/IC

Molecular Assembly and Magnetic Dynamics of Two Novel Dy_6 and Dy_8 Aggregates

Yun-Nan Guo,[†,‡] Xiao-Hua Chen,[§] Shufang Xue,[†,‡] and Jinkui Tang*[,†]

[†]State Key Laboratory of Rare Earth Resource Utilization, Changchun Institute of Applied Chemistry, Chinese Academy of Sciences, Changchun 130022, People's Republic of China

[‡]Graduate School of the Chinese Academy of Sciences, Beijing 100039, People's Republic of China

[§]College of Chemistry and Materials Science, Fujian Normal University, Fuzhou 350007, People's Republic of China

Supporting Information

ABSTRACT: Complexation of dysprosium(III) with the heterodonor chelating ligand *o*-vanillin picolinoylhydrazone (H_2ovph) in the presence of a carbonato ligand affords two novel Dy_6 and Dy_8 clusters, namely, $[Dy_6(ovph)_4(Hpvph)_2Cl_4(H_2O)_2(CO_3)_2]\cdot CH_3OH\cdot H_2O\cdot CH_3CN$ (**2**) and $[Dy_8(ovph)_8(CO_3)_4(H_2O)_8]\cdot 12CH_3CN\cdot 6H_2O$ (**3**). Compound **2** is composed of three petals of the Dy_2 units linked by two carbonato ligands, forming a triangular prism arrangement, while compound **3** possesses an octanuclear core with an unprecedented tub conformation, in which Dy(ovph) fragments are attached to the sides of the carbonato core. The static and dynamic magnetic properties are reported and discussed. In the Dy_6 aggregate, three Dy_2 "skeletons", having been well preserved (see the scheme), contribute to the single-molecule-magnet behavior with a relatively slow tunneling rate, while the Dy_8 cluster only exhibits a rather small relaxation barrier.

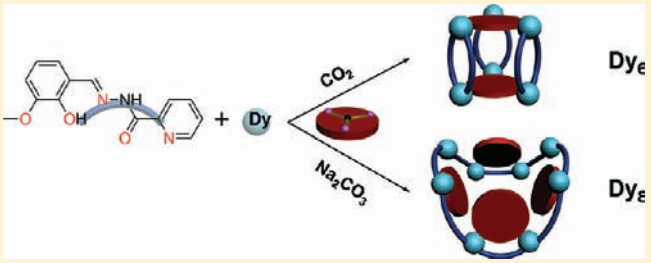

INTRODUCTION

Synthesis is the pivot of chemistry. A renovated subject of nanoscale magnetic materials focuses on the synthesis of single-molecule magnets (SMMs), where slow relaxation and quantum tunneling of the magnetization is purely of molecular origin.[1] This area thus represents a molecular, "bottom-up" approach to nanoscale magnets, complementary to the standard "top-down" approaches to nanoparticles of traditional magnetic materials[2] such as certain metals and metal oxides (e.g., Fe, Fe_3O_4, CrO_2). Recently, particular emphasis has been placed on the design of new SMMs applying 4f metal ions,[3] as a result of their significant magnetic anisotropy arising from the large, unquenched orbital angular momentum. The utility of the Dy^{III} ion as a vital candidate becomes apparent in this respect. The remarkable achievement has been the slow relaxation behavior first brought about by the toroidal arrangement of the local magnetization vector in a triangular Dy_3 cluster in spite of its almost nonmagnetic ground state.[4] Since then, successive pure dysprosium(III) SMMs within diverse network topologies have been described in the literature and yielded a flood of groundbreaking results: the highest relaxation energy barriers for multinuclear clusters[5] and the high blocking temperature.[6] From the standpoint of nuclearity, complexes of dysprosium(III) with up to 26 metal ions that exhibit slow relaxation of the magnetization have been reported.[7]

The design of coordination chemistry assemblies represents a promising avenue for the construction of functional SMMs. In this context, we have been engaged for years in the design of ligands to form molecules displaying distinct anisotropic centers through assembly with Dy^{III} ions.[5c,8] A further aim is to develop synthetic methodologies for acquiring molecular entities that fulfill the requirements of investigating the relaxation dynamics of lanthanide aggregates.[9] Thereinto, a peculiar paradigm comes out, over an asymmetric dinuclear dysprosium(III) SMM, $[Dy_2ovph_2Cl_2(MeOH)_3]\cdot MeCN$ (**1**), assembled by a rigid $ovph^{2-}$ ligand (H_2ovph = *o*-vanillin picolinoylhydrazone),[8b] in which the high axiality and Ising exchange interaction efficiently suppress quantum tunneling of the magnetization.

Scheme 1. (Top) Highly Axial Dy_2 SMM Building Block and (Bottom) Representation of the Self-assembly of Dy_6 and Dy_8 Aggregates Linked by Carbonato Ligands

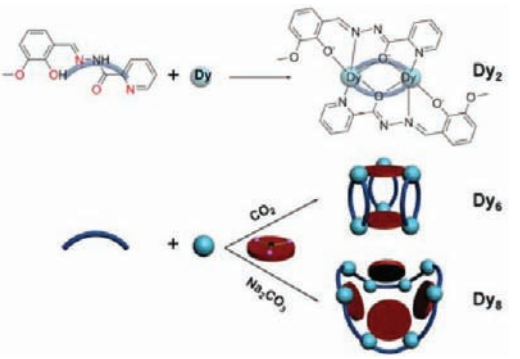

Received: October 6, 2011
Published: March 20, 2012

dx.doi.org/10.1021/ic202170z | *Inorg. Chem.* 2012, 51, 4035−4042

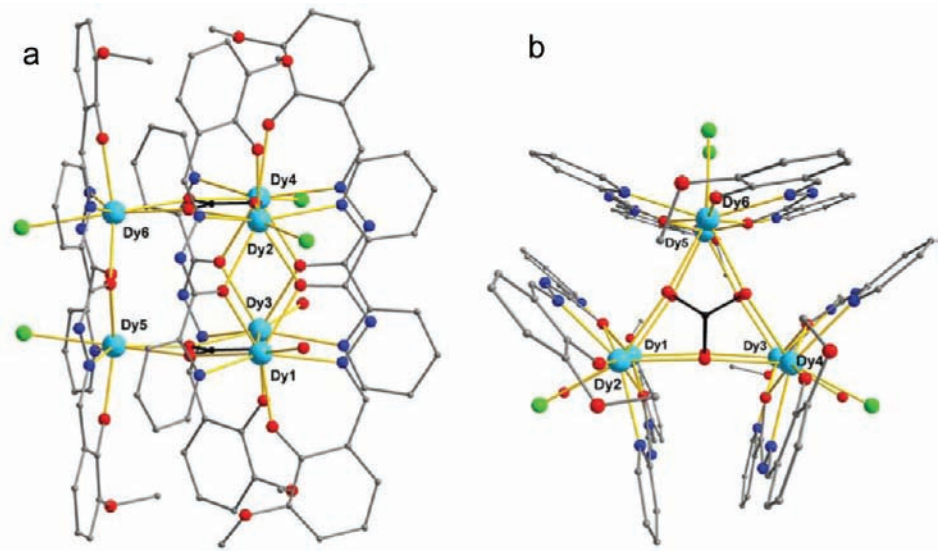

Figure 1. Side view (a) and top view (b) of the molecular structure of **2**. Hydrogen atoms and solvent molecules are omitted for clarity. Color scheme: sky blue, Dy; red, O; blue, N; green, Cl; gray, C.

Thus, such cluster can be regarded as highly axial lanthanide SMM building block, which may be responsible for the design of other efficient polynuclear SMMs (Scheme 1). With the goal of elaborating molecular nanoclusters, in the present work, new attempts to link magnetic Dy_2 building blocks into larger molecules were carried out by the use of the carbonato ligand with potential versatile coordination modes. When carbonate was deliberately introduced to the Dy^{III} and H_2ovph reaction mixture in the presence of triethylamine, they successfully furnish a hexanuclear complex, $[Dy_6(ovph)_4(Hpvph)_2Cl_4(H_2O)_2(CO_3)_2]\cdot CH_3OH\cdot H_2O\cdot CH_3CN$ (**2**), with a triangular prism arrangement and an octanuclear complex, $[Dy_8(ovph)_8(CO_3)_4(H_2O)_8]\cdot 12CH_3CN\cdot 6H_2O$ (**3**), with a tub conformation, in which Dy(ovph) fragments are attached to the sides of the carbonato core (Scheme 1). More interestingly, the crystals fall into two categories depending on the different sources of carbonate in the reaction mixture: crystals of **2** were formed by the feeding of CO_2, whereas crystals of **3** assembled in the presence of sodium carbonate. The static and dynamic magnetic properties are reported and discussed. In the Dy_6 aggregate, three Dy_2 "skeletons", having been well preserved (Scheme 1), contribute to the SMM behavior with a relatively slow tunneling rate, while the Dy_8 cluster only exhibits a rather small relaxation barrier.

EXPERIMENTAL SECTION

General Procedures. All chemicals were of reagent grade and were used without any further purification. Elemental analysis for C, H, and N were carried out on a Perkin-Elmer 2400 analyzer. Fourier transform infrared (FTIR) spectra were recorded with a Perkin-Elmer FTIR spectrophotometer using the reflectance technique (4000−300 cm^{-1}). Samples were prepared as KBr disks. Magnetic susceptibility measurements were performed in the temperature range 2−300 K, using a Quantum Design MPMS XL-7 SQUID magnetometer equipped with a 7 T magnet. The magnetization isotherm was collected at 1.9 K between 0 and 7 T. Samples were restrained in eicosane to prevent torquing. The diamagnetic corrections for the compounds were estimated using Pascal's constants,[10] and magnetic data were corrected for diamagnetic contributions of the sample holder.

Table 1. Crystallographic Data and Structure Refinement for Complexes 2 and 3

	2	3
formula	$C_{89}H_{81}Cl_4Dy_6N_{19}O_{28}$	$C_{140}H_{152}Dy_8N_{36}O_{50}$
M_r	2981.53	4438.98
cryst size [mm]	0.25 × 0.21 × 0.18	0.25 × 0.22 × 0.20
color	yellow blocks	red blocks
cryst syst	monoclinic	monoclinic
space group	$P2_1/n$	$C2/c$
T [K]	191(2)	191(2)
a [Å]	17.8984(8)	31.1933(13)
b [Å]	27.6222(12)	18.4912(7)
c [Å]	25.0228(11)	29.0411(11)
α [deg]	90	90
β [deg]	92.8880(10)	97.1320(10)
γ [deg]	90	90
V [Å ^{3}]	12355.4(9)	16621.3(11)
Z	4	4
D_{calcd} [g cm^{-3}]	1.603	1.774
μ(Mo Kα) [mm^{-1}]	0.71073	0.71073
F(000)	5744	8688
reflns collected	63574	45895
unique reflns	21910	16438
R_{int}	0.0700	0.0341
param/restraints	1289/4	991/0
GOF	0.997	1.048
R1 [$I > 2\sigma(I)$]	0.0600	0.0352
wR2 (all data)	0.2085	0.1015
largest diff peak/hole [e Å^{-3}]	2.531, −1.204	2.339, −0.894

Synthesis of H_2ovph. The Schiff-base ligand H_2ovph is synthesized by the condensation of picolinoyl hydrazide and *o*-vanillin in a 1:1 ratio in methanol according to the reported procedure.[11]

Synthesis of $[Dy_6(ovph)_4(Hpvph)_2Cl_4(H_2O)_2(CO_3)_2]\cdot CH_3OH\cdot H_2O\cdot CH_3CN$ (2). A suspension of $DyCl_3\cdot 6H_2O$ (0.2 mmol, 75.4 mg) and H_2ovph (54.2 mg, 0.2 mmol) in MeOH/CH_3CN (5 mL/10 mL) was treated with Et_3N (1.0 mmol, 0.14 mL). Then, CO_2 was bubbled into the reaction mixture (30 s), and the suspended reaction mixture gradually turned to a clear solution, which was stirred for 6 h and then left undisturbed to allow slow evaporation of the solvent. Yellow block-shaped single crystals of **2**, suitable for X-ray

dx.doi.org/10.1021/ic202170z | Inorg. Chem. 2012, 51, 4035−4042

diffraction analysis, formed after 1 week. Yield: 23 mg (23.1% based on the metal salt). Anal. Calcd (found) for $C_{89}H_{81}Cl_4N_{19}O_{28}Dy_6$: C, 35.85 (35.77); H, 2.74 (2.73); N, 8.93 (8.89). IR (KBr, cm^{-1}): 3446(br), 2837(w), 1620(s), 1552(s), 1545(w), 1457(m), 1437(m), 1352(w), 1317(m), 1287(w), 1245(s), 1220(m), 1171(w), 1089(s), 1054(w), 1021(w), 971(w), 935(w), 868(w), 812(w), 789(w), 745(m), 696(m), 635(m), 544(w).

Synthesis of $[Dy_8(ovph)_8(CO_3)_4(H_2O)_8]\cdot 12CH_3CN\cdot 6H_2O$ (3). Complex **3** was prepared in a manner similar to that of **2**, using $Na_2CO_3\cdot 10H_2O$ instead of feeding CO_2. A suspension of $DyCl_3\cdot 6H_2O$ (0.2 mmol, 75.4 mg) and H_2ovph (54.2 mg, 0.2 mmol) in MeOH/CH_3CN (5 mL/10 mL) was treated with Et_3N (1.0 mmol, 0.14 mL). Then, $Na_2CO_3\cdot 10H_2O$ (85.8 mg, 0.3 mmol) was added into the reaction mixture. The reaction mixture was stirred 6 h and subsequently filtered. The yellow filtrate was left undisturbed to allow slow evaporation of the solvent. Red block-shaped single crystals of **3**, suitable for X-ray diffraction analysis, formed after 1 month. Yield: 58 mg (52% based on the metal salt). Anal. Calcd (found) for $C_{140}H_{152}N_{36}O_{50}Dy_8$: C, 37.85 (37.74); H, 3.42 (3.40); N, 11.35 (11.31). IR (KBr, cm^{-1}): 3381(br), 2993(w), 2928(w), 2829(w), 1609(s), 1552(s), 1534(s), 1477(s), 1463(m), 1451(s), 1418(w), 1399(w), 1349(s), 1241(m), 1217(s), 1166(w), 1109(w), 1081(w), 1049(w), 1011(w), 972(w), 921(w), 869(w), 847(w), 803(w), 784(w), 747(w), 734(m), 714(w), 694(w), 634(w), 424(w).

RESULTS AND DISCUSSION

The reactions with different sources of carbonate (CO_2 or Na_2CO_3) generate distinct compounds which is most likely due to the different acidity of the respective solutions.

Compound 2. The reaction of dysprosium chloride with H_2ovph in the mixture of methanol, acetonitrile, and triethylamine, by feeding CO_2, produces the Dy_6 cluster **2**, whose molecular structure is depicted in Figure 1. Compound **2** is crystallized in the monoclinic space group $P2_1/n$ with $Z = 4$. Details for the structure solution and refinement are summarized in Table 1, and selected bond distances and angles are listed in Table 2. The Dy_6 structure can be considered as resulting from the formal linkage by two carbonato ligands of three petals of the Dy_2 units in **1** with the concomitant formal loss of the terminal ligands (Figure 2, a and b). The metal centers in each Dy_2 petal are bridged by the alkoxido groups (O1 and O4 in Figure 2a) of two antiparallel, or "head-to-tail" $ovph^{2-}$/$Hovph^{-}$ ligands, with an average Dy···Dy distance being 3.860 Å and an average Dy−O−Dy angle 111.7°, which are in agreement with the corresponding values 3.864 Å and 111.9° in the parent compound **1**.[8b] The pyridyl nitrogen atoms (N3 and N6, take the Dy1···Dy2 petal as an example; Figure 2a), the hydrazide nitrogen atoms (N1 and N4), and the phenolate

Table 2. Selected Bond Distances (Å) and Angles (deg) in Complexes 2 and 3[a]

Compound **2**							
Dy1−O1	2.144(9)	Dy1−O3	2.314(8)	Dy1−O6	2.322(8)	Dy1−O19	2.458(9)
Dy1−O22	2.438(8)	Dy1−O25	2.509(9)	Dy1−N1	2.461(10)	Dy1−N6	2.519(11)
Dy2−O3	2.352(9)	Dy2−O4	2.136(9)	Dy2−O6	2.328(8)	Dy2−O20	2.464(8)
Dy2−O21	2.446(8)	Dy2−N3	2.512(10)	Dy2−N4	2.467(11)	Dy2−Cl1	2.724(4)
Dy3−O7	2.140(10)	Dy3−O9	2.330(9)	Dy3−O12	2.326(9)	Dy3−O19	2.456(9)
Dy3−O23	2.453(8)	Dy3−O26	2.464(10)	Dy3−N7	2.462(11)	Dy3−N12	2.529(11)
Dy4−O9	2.348(9)	Dy4−O10	2.138(10)	Dy4−O12	2.329(9)	Dy4−O20	2.497(9)
Dy4−O24	2.424(8)	Dy4−N9	2.534(12)	Dy4−N10	2.459(11)	Dy4−Cl2	2.711(5)
Dy5−O13	2.145(9)	Dy5−O15	2.337(8)	Dy5−O18	2.341(8)	Dy5−O22	2.431(8)
Dy5−O23	2.472(7)	Dy5−N13	2.480(10)	Dy5−N18	2.517(11)	Dy5−Cl3	2.637(5)
Dy6−O15	2.345(8)	Dy6−O16	2.164(9)	Dy6−O18	2.316(8)	Dy6−O21	2.434(8)
Dy6−O24	2.449(8)	Dy6−N15	2.508(10)	Dy6−N17	2.455(10)	Dy6−Cl4	2.703(6)
Dy1−Dy2	3.8625(9)	Dy3−Dy4	3.8493(10)	Dy5−Dy6	3.8670(8)		
Dy1−O3−Dy2	111.7(3)	Dy1−O6−Dy2	112.3(3)	Dy3−O9−Dy4	110.7(3)		
Dy3−O12−Dy4	111.6(3)	Dy5−O15−Dy6	111.4(3)	Dy5−O18−Dy6	112.3(3)		
Dy1−O19−Dy3	168.9(4)	Dy1−O22−Dy5	168.2(4)	Dy2−O20−Dy4	170.0(4)		
Dy2−O21−Dy6	168.6(4)	Dy3−O23−Dy5	167.9(4)	Dy4−O24−Dy6	168.5(4)		
O19−Dy1−O22	53.9(3)	O20−Dy2−O21	53.6(3)	O19−Dy3−O23	53.9(3)		
O20−Dy4−O24	53.6(3)	O22−Dy5−O23	53.8(3)	O21−Dy6−O24	54.1(3)		
Compound **3**							
Dy1−O1	2.339(4)	Dy1−O2	2.207(4)	Dy1−O4	2.371(4)	Dy1−O13	2.379(4)
Dy1−O17	2.331(4)	Dy1−O20	2.310(4)	Dy1−N3	2.474(5)	Dy1−N4	2.603(5)
Dy2−O4	2.419(4)	Dy2−O5	2.249(4)	Dy2−O7	2.448(4)	Dy2−O14	2.420(4)
Dy2−O17	2.511(4)	Dy2−O18	2.385(4)	Dy2−O21	2.439(4)	Dy2−N6	2.501(5)
Dy2−N7	2.653(5)	Dy3−O7	2.347(4)	Dy3−O8	2.197(4)	Dy3−O10	2.359(4)
Dy3−O15	2.365(4)	Dy3−O18	2.309(4)	Dy3−O22#1	2.330(4)	Dy3−N9	2.475(5)
Dy3−N10	2.589(5)	Dy4−O1#1	2.467(4)	Dy4−O10	2.403(4)	Dy4−O11	2.261(4)
Dy4−O16	2.434(4)	Dy4−O19	2.417(4)	Dy4−O20#1	2.382(4)	Dy4−O22#1	2.517(4)
Dy4−N1#1	2.654(5)	Dy4−N12	2.505(5)	Dy1−Dy2	3.9808(4)	Dy1−Dy4#1	3.9820(4)
Dy2−Dy3	3.9756(4)	Dy3−Dy4	3.9709(4)	Dy4−Dy1#1	3.9820(4)		
Dy1−O4−Dy2	112.43(15)	Dy1−O17−Dy2	110.54(14)	Dy2−O7−Dy3	111.99(15)		
Dy2−O18−Dy3	115.76(15)	Dy3−O10−Dy4	113.01(15)	Dy3−O22−Dy4	109.98(15)		
Dy1−O1−Dy4#1	111.87(15)	Dy1−O20−Dy4#1	116.11(15)				

[a]Symmetry codes: #1, $-x + 1, y, -z + {}^1/_2$.

dx.doi.org/10.1021/ic202170z | Inorg. Chem. 2012, 51, 4035−4042

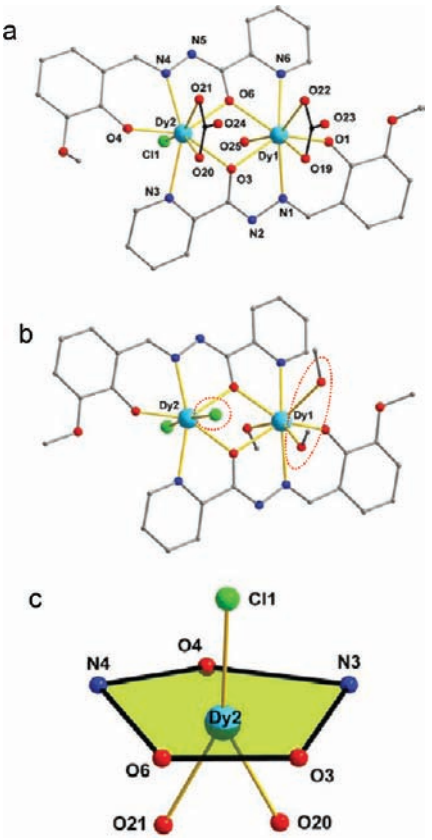

Figure 2. (a) Structure of the Dy1···Dy2 petal in **2**. Hydrogen atoms are omitted for clarity. (b) Formal formation of the Dy1···Dy2 petal by linking two CO_3^{2-} anions in complex **1**, by the loss of one terminal chloride ion and two methanol ligands (red circles). (c) Hula-hoop-like geometry for Dy2 with the cyclic ring (hula hoop) defined by the atoms N3, O3, O6, N4, and O4.

oxygen atoms (O1 and O6) of the ovph^{2-}/Hovph^{-} ligands also coordinate to the dysprosium centers. The charge balance requires that two phenolate oxygen atoms (O4 and O13) in two Hovph^{-} ligands remain protonated, in which O4−C15 [1.329(17) Å] and O13−C57 [1.339(16) Å] are slightly longer than another four O(phenolate)−C bands (average 1.308 Å) in fully deprotonated states.

In the core of the molecule, each of two carbonato ligands binds three dysprosium ions with a rare μ_3-η_2:η_2:η_2-tridentate bridging mode.[12] As shown in Figure 1b, every vertex oxygen atom of the carbonato ligands acts as a donor unit with an angle of around 167°, and the Dy^{III} ion acts as an acceptor unit with an angle of around 54°. All Dy−O(carbonate) bonds are almost equal with an average bond length of 2.452 Å, which is obviously shorter than that of a lanthanide(III) species [Ln−O(carbonate) = 2.544 Å].[13] This has been justified with the lanthanide contraction, i.e., with a decrease in the ionic radius from La^{III} to Dy^{III}. The bridging mode makes the carbon atoms of CO_3^{2-} lie on the triangular prism quasi-C_3 axis and the CO_3^{2-} ligands symmetrically fixed in the center of the cluster (Scheme 1). From another point of view, the presence of the carbonato core as a seed is critical for the formation of crystals. Additional peripheral coordination is provided by four Cl^{-} anions and two water molecules. Consequently, all of the Dy^{III} centers have an eight-coordinate sphere exhibiting a hula-hoop-like geometry whose cyclic ring (hula hoop) is shaped by the stereochemical preferences of two ovph^{2-}/Hovph^{-} ligands (Figure 2c).[14]

Compound 3. The procedure was the same as that for **2** except $Na_2CO_3{\cdot}10H_2O$ was used in place of CO_2, which produces the Dy_8 cluster **3**. X-ray crystallographic studies revealed that the crystal belonged to the monoclinic space group *C*2/*c*. A perspective view of complex **3** is represented in Figure 3.

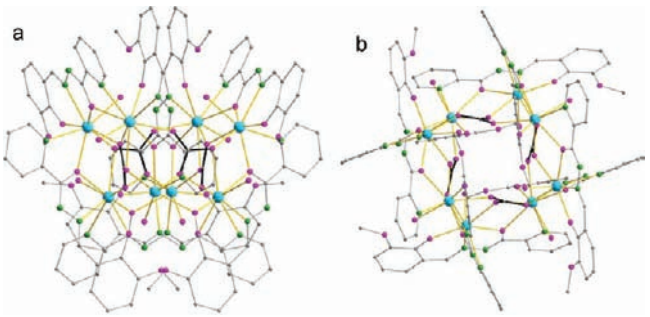

Figure 3. Side view (a) and top view (b) of the molecular structure of **3**. Hydrogen atoms and solvent molecules are omitted for clarity. Color scheme: sky blue, Dy; pink, O; green, N; gray, C.

The whole Dy_8 cluster exhibits C_2 crystallographic symmetry. The asymmetric unit containing a trapezoid arrangement of four Dy^{III} ions (Dy1−Dy4) and four linking ovph^{2-} ligands constructs a supramolecular hemisphere (Figure 4a). When crystallographic 2-fold symmetry is applied to the asymmetric unit, two hemispheres fuse to manufacture a spherical molecule with a diameter of ca. 1.8 nm.

The eight metal atoms are arranged in an interesting topology: the complex possesses a $[Dy_8(\mu_4\text{-}CO_3^{2-})_4(\mu_2\text{-}O)_8]$ core, and the dysprosium atoms adopt a tub conformation (Figure 4b), akin to the cyclooctatetraene molecule, with Dy···Dy distances that range between 3.9709(4) and 3.9820(4) Å. The resulting core structure is unique in lanthanide(III) chemistry. This tub conformation can be considered as two nearly parallel Dy_4 planes (Dy1, Dy4, Dy1A, Dy4A and Dy2, Dy3 Dy2A, Dy3A), between which four CO_3^{2-} anions are sandwiched. Each carbonato ligand binds to four adjacent metal centers with a chelating and bridging configuration. Overall, the coordination mode is μ_4-η_1:η_2:η_1:η_1. Along each side of the tub, a deprotonated ovph^{2-} ligand bridges two Dy^{III} ions by its alkoxido atom (O1, O4, O7, and O10 in Figure 4a) with Dy−O−Dy angles of 111.87(15)−113.01(15)°. For each Dy^{III} ion, one water molecule is required to complete the respective coordination numbers, making it eight-coordinate for Dy1 and Dy3 and nine-coordinate for Dy2 and Dy4. Moreover, the coordinated water forms hydrogen bonds among *o*-vanillin groups of ovph^{2-} ligands and leaves no void space.

Magnetic Properties of 2. The direct-current (dc) magnetic susceptibility of **2** has been measured in an applied magnetic field of 1000 Oe in the temperature range 300−2 K and can be seen plotted as $\chi_M T$ versus T in Figure 5. The $\chi_M T$ value at 300 K of 82.1 cm^3 K mol^{-1} is lower than the expected value of 85.02 cm^3 K mol^{-1} for six uncoupled Dy^{III} ions ($S = {}^5/_2$, $L = 5$, $^6H_{15/2}$, and $g = {}^4/_3$), and it gradually decreases with decreasing temperature until 20 K. There is then a small maximum as the temperature falls further (75.3 cm^3 K mol^{-1} at 6 K), before a further rapid fall at the lowest temperature studied. The Stark sublevels of the anisotropic Dy^{III} ions are thermally depopulated when the temperature is lowered, resulting in a decrease of the $\chi_M T$ product at the high-temperature

dx.doi.org/10.1021/ic202170z | *Inorg. Chem.* 2012, 51, 4035−4042

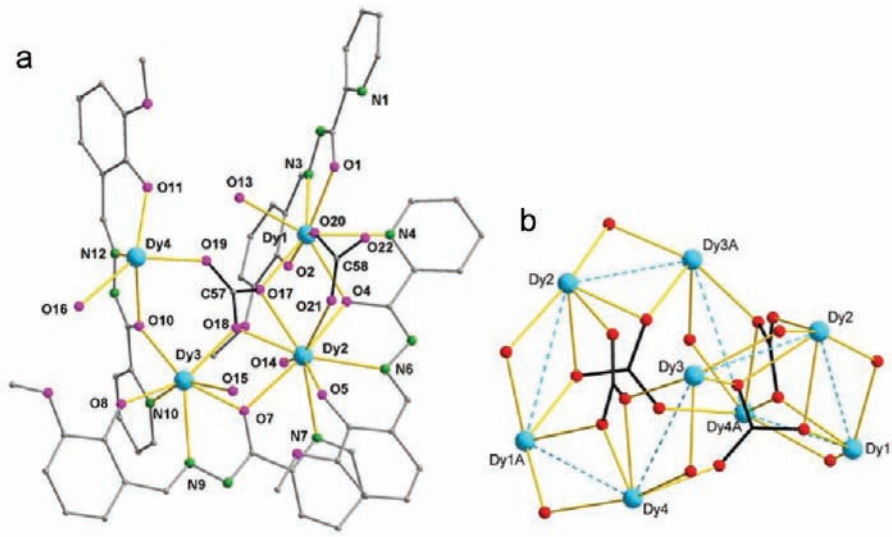

Figure 4. (a) Crystallographic asymmetric unit of **3**, which is half of the whole assembly as a result of crystallographic 2-fold symmetry. (b) Core structure of **3**. All Dy^{III} ions are bridged by oxygen atoms and form a tub conformation (dashed lines).

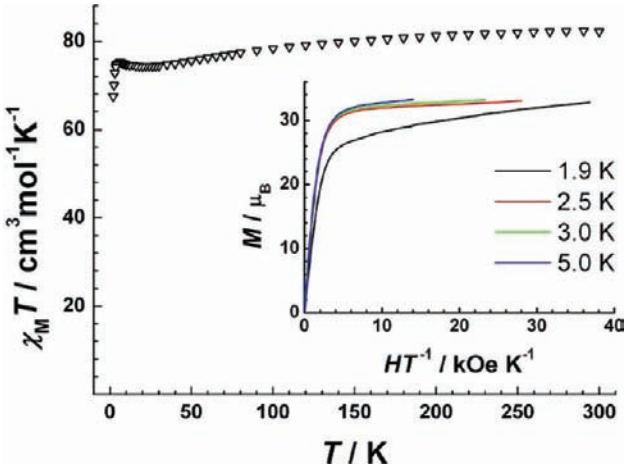

Figure 5. Temperature dependence of the $\chi_M T$ product at 1000 Oe and field dependence of the magnetization at low temperatures (inset) for **2**.

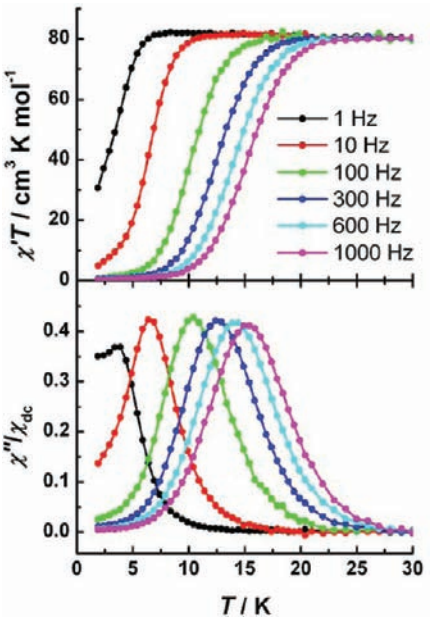

Figure 6. Temperature dependence of the ac magnetic susceptibility for complex **2** of the imaginary component (bottom) and $\chi'T$ product (top) in zero static field. The χ'' data are normalized at each temperature by the corresponding value of χ_{dc}.

range, and the maximum is probably due to the presence of an intramolecular ferromagnetic interaction between the metal ions, as observed in the parent complex **1**. A residual slope is observed at high field (>60 kOe) on the *M* versus *H* data (inset of Figure 5), indicating failure of the magnetization to saturate and some anisotropy and/or low-lying excited states in the system.

The dynamics of the magnetization were investigated using alternating-current (ac) susceptibility measurements, with the results in zero static field given in Figure 6. Each $\chi'T$ value exhibits a sudden decrease with decreasing *T* depending on the ac frequency, signaling the "freezing" of the spins by the anisotropy barrier. This is accompanied by a frequency-dependent out-of-phase (χ'') signal. In the bottom panel of Figure 6, the χ'' curves were divided by the dc susceptibility χ_{dc}, so that the relaxation time τ matches the inverse of the angular frequency ω exactly at the peak temperature of the corresponding curve, where the $\chi'T$ dispersion curve is observed.[15] χ''/χ_{dc} signal is observed with a maximum at 15 K for 1000 Hz, which shifts to the low-temperature regime as the frequencies decrease to 1 Hz. All of these features are indicative of slow relaxation of the molecular magnetization and, hence, of SMM behavior. This allows us to monitor the relaxation process over a large temperature range under zero static field.

The magnetization relaxation time (τ) can be simultaneously derived from the temperature (Figure 6) and frequency dependence of the ac susceptibility (Figure S1 in the Supporting Information) and plotted as a function of $1/T$ in Figure 7. The data of the high-temperature range (11−20 K) nicely follow a thermally activated behavior [Arrhenius law, $\tau = \tau_0 \exp(U_{eff}/kT)$] with an effective energy barrier U_{eff}, of 76 K and a preexponential factor, τ_0, of 1.2×10^{-6} s. At lower temperatures, τ becomes weakly dependent on *T* and reaches 0.2 s as the temperature approaches 1.9 K. This behavior shows a crossover from a thermally activated Orbach mechanism that

dx.doi.org/10.1021/ic202170z | Inorg. Chem. 2012, 51, 4035−4042

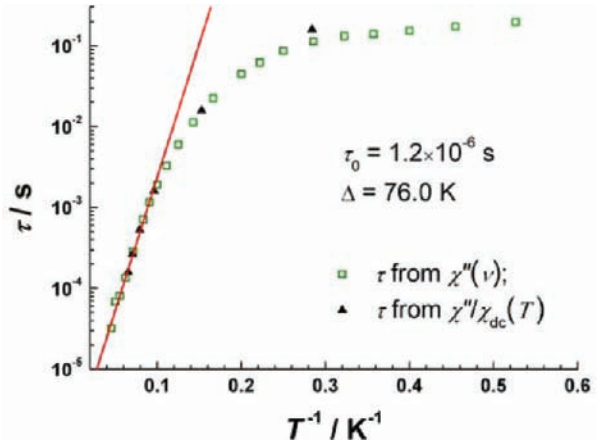

Figure 7. Magnetization relaxation time τ versus T^{-1} plot for **2** under zero dc field. The line is fitted with the Arrhenius law.

is predominant at high temperature to a quantum tunneling relaxation pathway taking over at $T < 10$ K. At low enough temperature, the exchange interaction between the metal sites is an important factor for blockage of the magnetization in the weak exchange limit, which may lead to a relatively slow tunneling rate (>0.2 s).[8b,16]

The data plotted as Cole−Cole plots show a perfectly symmetrical shape (Figure 8), which is particularly useful to

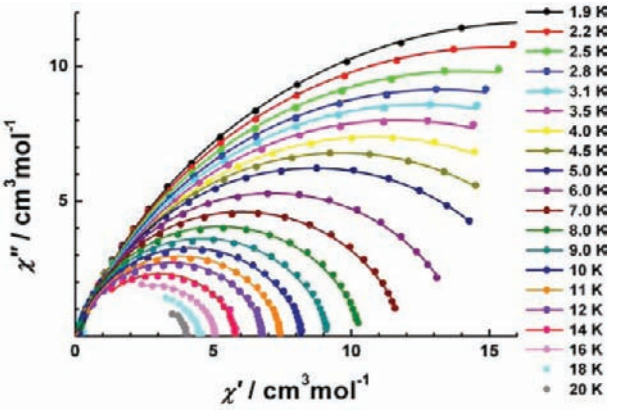

Figure 8. Cole−Cole plots measured below 20 K and zero dc field. The lines represent the best-fit calculated values for each temperature with an extended Debye model with α parameters below 0.23.

quantify the width distribution of the relaxation rate by introducing the α parameter in the Debye formula ($\alpha = 0$ for a Debye model).[1a] Such a symmetrical shape is remarkable because lanthanide systems often feature a very broad distribution[16,17] or an asymmetrical Cole−Cole plot[8c,18] in the low-temperature regime, while **2** displays a narrow distribution: only a moderate increase of the dispersion upon lowering T, with a passing from $\alpha = 0.1$ at 16 K to 0.23 at 1.9 K (Table S1 in the Supporting Information). Here, the dominance of a single relaxation process agrees with the presence of a unique coordination sphere of Dy^{III} ion in **2**, which is different from the presence of two closely spaced relaxation processes in the parent compound **1** due to its asymmetric Dy_2 unit.

Magnetic Properties of 3. The dc magnetic susceptibility studies of **3** were carried out in an applied magnetic field of 1000 Oe in the temperature range 300−2 K. As shown in Figure 9, the $\chi_M T$ value of 107.4 cm^3 K mol^{-1} at room

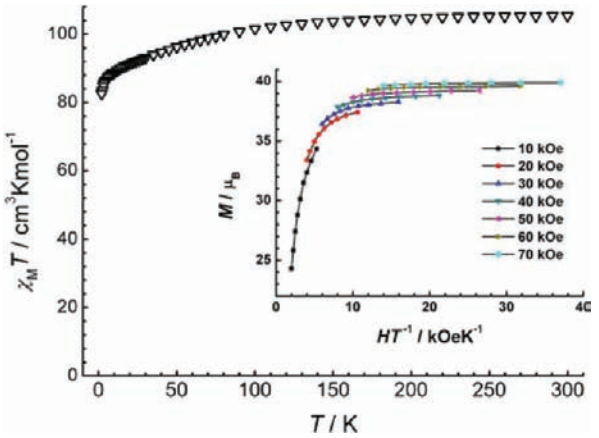

Figure 9. Plot of $\chi_M T$ versus T for **3**. The inset is a plot of the reduced magnetization M versus H/T. The solid lines are eye guides.

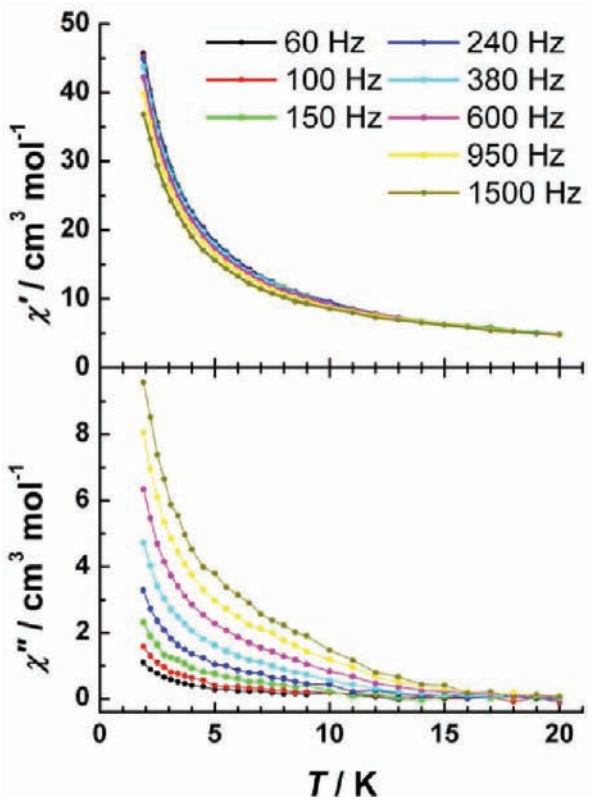

Figure 10. Temperature dependence of the in-phase (top) and out-of-phase (bottom) ac susceptibilities for **3** under zero dc field.

temperature is lower than the expected value of 113.4 cm^3 K mol^{-1} for eight uncoupled Dy^{III} ions. The $\chi_M T$ product remains roughly constant with decreasing temperature down to 100 K and then gradually decreases and further drops to a minimum value of 82.6 cm^3 K mol^{-1} at 2 K, which may be ascribed to the progressive depopulation of excited Stark sublevels of the Dy^{III} ions, even if some other effects like the weak exchange interaction between spin carriers or magnetic anisotropy might also partially induce deviation of the Curie law.[19] Magnetization data were collected in the 10−70 kOe field range and 1.9−4 K temperature range. The nonsuperimposition M versus H/T data on a single master curve (inset of Figure 9) indicates the effects arising from magnetic anisotropy.

dx.doi.org/10.1021/ic202170z | Inorg. Chem. 2012, 51, 4035−4042

The low-temperature ac susceptibility also shows slow magnetic relaxation phenomena for **3** (Figure 10). The χ'' component of the susceptibility exhibits frequency dependence below 15 K down to the lowest measured temperature of 1.9 K. The ratio of the intensities of the out-of-phase and in-phase signals is about 1:4 at 1.9 K and 1500 Hz. In well-established SMMs, this ratio is normally approximately 1:1 at T_{max} of χ''. The observed behavior in **3** suggests that maxima lie below the operating minimum temperature (1.9 K) or above the obtained maximum frequency (1500 Hz) of our SQUID instrument. These behaviors suggest **3** to possibly be a Dy^{III} SMM but one with a rather small relaxation barrier.[20] The absence of frequency-dependent peaks in out-of-phase susceptibility signals may be caused by the presence of a relatively fast zero-field relaxation. ac data have also been recorded under a small dc field in order to suppress possible fast zero-field quantum relaxation (Figure 11). The application of the fields of 50, 100, and 200 Oe, however, has practically no effect on the ac signal profile, suggesting that tunneling in zero field is not an efficient pathway above 1.9 K.[5e,19]

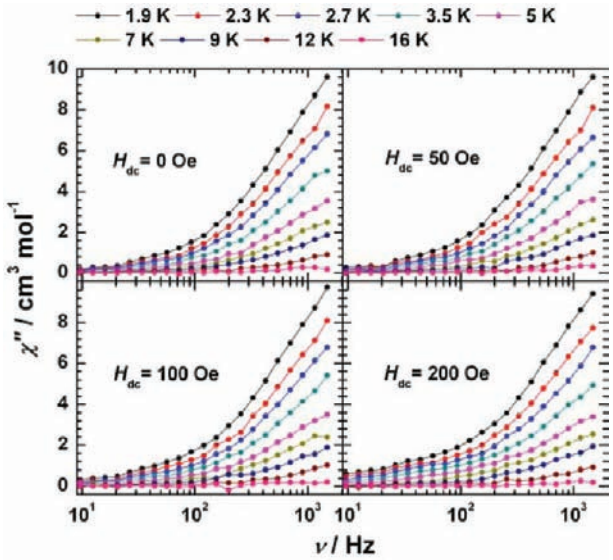

Figure 11. Frequency-dependent out-of-phase component of the ac susceptibility of **3** under dc fields of 0, 50, 100, and 200 Oe, showing an inefficient tunneling pathway in zero field above 1.9 K.

CONCLUSION

We have assembled two pure polynuclear dysprosium(III) clusters using the Dy(ovph) building blocks and the versatile carbonato linker. Compound **2** is composed of three petals of the Dy_2 units linked by two carbonato ligands, forming a triangular prism arrangement, while compound **3** possesses an octanuclear core with an unprecedented tub conformation, in which Dy(ovph) fragments are attached to the sides of the carbonato core (Scheme 1). Both of these two dysprosium(III) complexes exhibit SMM behavior. While compound **3** shows a rather small relaxation barrier, in compound **2**, three well-preserved Dy_2 "skeletons" contribute to the SMM behavior with a relatively slow tunneling rate. By virtue of the assembly of **2** and **3**, we have verified that the use of highly axial single-lanthanide building blocks is a convenient strategy for the design of molecular architectures with the appropriate structure to further exploit their functional properties.

ASSOCIATED CONTENT

Supporting Information

X-ray crystallographic data in CIF format, relaxation fitting parameters (Table S1), and magnetic measurement (Figure S1). This material is available free of charge via the Internet at http://pubs.acs.org.

AUTHOR INFORMATION

Corresponding Author

*E-mail: tang@ciac.jl.cn.

ACKNOWLEDGMENTS

We thank the National Natural Science Foundation of China (Grants 20871113, 91022009, and 20921002) for financial support.

REFERENCES

(1) (a) Gatteschi, D.; Sessoli, R.; Villain, J. *Molecular Nanomagnets*; Oxford University Press: Oxford, U.K., 2006. (b) Aromí, G.; Brechin, E. K. *Struct. Bonding (Berlin)* **2006**, *122*, 1−67. (c) Bruce, D. W.; O'Hare, D.; Walton, R. I. *Molecular Materials (Inorganic Materials Series)*; John Wiley & Sons: Hoboken, NJ, 2010.

(2) Tasiopoulos, A. J.; Perlepes, S. P. *Dalton Trans.* **2008**, 5537−5555.

(3) (a) Sessoli, R.; Powell, A. K. *Coord. Chem. Rev.* **2009**, *253*, 2328−2341. (b) Lin, S.; Guo, Y.; Xu, G.; Tang, J. *Chin. J. Appl. Chem.* **2010**, *27*, 1365−1371. (c) Langley, S. K.; Chilton, N. F.; Gass, I. A.; Moubaraki, B.; Murray, K. S. *Dalton Trans.* **2011**, *40*, 12656−12659. (d) Andrews, P. C.; Beck, T.; Fraser, B. H.; Junk, P. C.; Massi, M.; Moubaraki, B.; Murray, K. S.; Silberstein, M. *Polyhedron* **2009**, *28*, 2123−2130. (e) Langley, S. K.; Moubaraki, B.; Forsyth, C. M.; Gass, I. A.; Murray, K. S. *Dalton Trans.* **2010**, *39*, 1705−1708.

(4) (a) Tang, J.; Hewitt, I.; Madhu, N. T.; Chastanet, G.; Wernsdorfer, W.; Anson, C. E.; Benelli, C.; Sessoli, R.; Powell, A. K. *Angew. Chem., Int. Ed.* **2006**, *45*, 1729−1733. (b) Chibotaru, L. F.; Ungur, L.; Soncini, A. *Angew. Chem., Int. Ed.* **2008**, *47*, 4126−4129. (c) Luzon, J.; Bernot, K.; Hewitt, I. J.; Anson, C. E.; Powell, A. K.; Sessoli, R. *Phys. Rev. Lett.* **2008**, *100*, 247205. (d) Ungur, L.; Heuvel, W. V. d.; Chibotaru, L. F. *New J. Chem.* **2009**, *33*, 1224−1230. (e) Salman, Z.; Giblin, S. R.; Lan, Y.; Powell, A. K.; Scheuermann, R.; Tingle, R.; Sessoli, R. *Phys. Rev. B* **2010**, *82*, 174427.

(5) (a) Blagg, R. J.; Muryn, C. A.; McInnes, E. J. L.; Tuna, F.; Winpenny, R. E. P. *Angew. Chem., Int. Ed.* **2011**, *50*, 6530−6533. (b) Watanabe, A.; Yamashita, A.; Nakano, M.; Yamamura, T.; Kajiwara, T. *Chem.—Eur. J.* **2011**, *17*, 7428−7432. (c) Guo, Y.-N.; Xu, G.-F.; Gamez, P.; Zhao, L.; Lin, S.-Y.; Deng, R.; Tang, J.; Zhang, H.-J. *J. Am. Chem. Soc.* **2010**, *132*, 8538−8539. (d) Lin, P. H.; Burchell, T. J.; Ungur, L.; Chibotaru, L. F.; Wernsdorfer, W.; Murugesu, M. *Angew. Chem., Int. Ed.* **2009**, *48*, 9489−9492. (e) Hewitt, I. J.; Tang, J.; Madhu, N. T.; Anson, C. E.; Lan, Y.; Luzon, J.; Etienne, M.; Sessoli, R.; Powell, A. K. *Angew. Chem., Int. Ed.* **2010**, *49*, 6352−6356.

(6) Rinehart, J. D.; Fang, M.; Evans, W. J.; Long, J. R. *Nat. Chem.* **2011**, *3*, 538−542.

(7) Gu, X. J.; Xue, D. F. *Inorg. Chem.* **2007**, *46*, 3212−3216.

(8) (a) Xue, S.; Zhao, L.; Guo, Y.-N.; Deng, R.; Guo, Y.; Tang, J. *Dalton Trans.* **2011**, *40*, 8347−8352. (b) Guo, Y.-N.; Xu, G.-F.; Wernsdorfer, W.; Ungur, L.; Guo, Y.; Tang, J.; Zhang, H.; Chibotaru, L. F.; Powell, A. K. *J. Am. Chem. Soc.* **2011**, *133*, 11948−11951. (c) Ke, H.; Xu, G.-F.; Guo, Y.-N.; Gamez, P.; Beavers, C. M.; Teat, S. J.; Tang, J. *Chem. Commun.* **2010**, 6057−6059. (d) Tian, H.; Zhao, L.; Guo, Y.-N.; Guo, Y.; Tang, J. *Chem. Commun.* **2012**, *48*, 708−710. (e) Tian, H.; Wang, M.; Zhao, L.; Guo, Y.-N.; Guo, Y.; Tang, J.; Liu, Z. *Chem.—Eur. J.* **2012**, *18*, 442−445.

(9) Guo, Y.-N.; Xu, G.-F.; Guo, Y.; Tang, J. *Dalton Trans.* **2011**, *40*, 9953−9963.

(10) Boudreaux, E. A.; Mulay, L. N. *Theory and Applications of Molecular Paramagnetism*; John Wiley & Sons: New York, 1976.

(11) Wang, D.; Liu, S. X. *Polyhedron* **2007**, *26*, 5469−5476.
(12) Chesman, A. S. R.; Turner, D. R.; Moubaraki, B.; Murray, K. S.; Deacon, G. B.; Batten, S. R. *Chem.—Eur. J.* **2009**, *15*, 5203−5207.
(13) Tang, X. L.; Wang, W. H.; Dou, W.; Jiang, J.; Liu, W. S.; Qin, W. W.; Zhang, G. L.; Zhang, H. R.; Yu, K. B.; Zheng, L. M. *Angew. Chem., Int. Ed.* **2009**, *48*, 3499−3502.
(14) (a) Runschke, C.; Meyer, G. *Z. Anorg. Allg. Chem.* **1997**, *623*, 1493−1495. (b) Ruiz-Martinez, A.; Casanova, D.; Alvarez, S. *Chem.—Eur. J* **2008**, *14*, 1291−1303.
(15) (a) Magnani, N.; Apostolidis, C.; Morgenstern, A.; Colineau, E.; Griveau, J.-C.; Bolvin, H.; Walter, O.; Caciuffo, R. *Angew. Chem., Int. Ed.* **2011**, *50*, 1696−1698. (b) Ishikawa, N.; Sugita, M.; Ishikawa, T.; Koshihara, S.-y.; Kaizu, Y. *J. Phys. Chem. B* **2004**, *108*, 11265−11271.
(16) Sharples, J. W.; Zheng, Y.-Z.; Tuna, F.; McInnes, E. J. L.; Collison, D. *Chem. Commun.* **2011**, *47*, 7650−7652.
(17) Bernot, K.; Pointillart, F.; Rosa, P.; Etienne, M.; Sessoli, R.; Gatteschi, D. *Chem. Commun.* **2010**, *46*, 6458−6460.
(18) Long, J.; Habib, F.; Lin, P.-H.; Korobkov, I.; Enright, G.; Ungur, L.; Wernsdorfer, W.; Chibotaru, L. F.; Murugesu, M. *J. Am. Chem. Soc.* **2011**, *133*, 5319−5328.
(19) Gamer, M. T.; Lan, Y. H.; Roesky, P. W.; Powell, A. K.; Clérac, R. *Inorg. Chem.* **2008**, *47*, 6581−6583.
(20) Papatriantafyllopoulou, C.; Stamatatos, T. C.; Efthymiou, C. G.; Cunha-Silva, L.; Paz, F. A. A.; Perlepes, S. P.; Christou, G. *Inorg. Chem.* **2010**, *49*, 9743−9745.